Hindawi
Advances in Materials Science and Engineering
Volume 2018, Article ID 3792672, 7 pages
https://doi.org/10.1155/2018/3792672

Research Article

Stable Cu_2O Photoelectrodes by Reactive Ion Beam Sputter Deposition

Ching-Hsiu Chen, Assamen Ayalew Ejigu, and Liang-Chiun Chao

Graduate Institute of Electro-Optical Engineering, Department of Electronic and Computer Engineering, National Taiwan University of Science and Technology, Taipei 106, Taiwan

Correspondence should be addressed to Liang-Chiun Chao; lcchao@mail.ntust.edu.tw

Received 8 March 2018; Revised 8 June 2018; Accepted 10 June 2018; Published 24 September 2018

Academic Editor: José A. Correia

Cu_2O has been deposited on quartz substrates by reactive ion beam sputter deposition. Experimental results show that by controlling argon/oxygen flow rates, both n-type and p-type Cu_2O samples can be achieved. The bandgap of n-type and p-type Cu_2O were found to be 2.3 and 2.5 eV, respectively. The variable temperature photoluminescence study shows that the n-type conductivity is due to the presence of oxygen vacancy defects. Both samples show stable photocurrent response that photocurrent change of both samples after 1,000 seconds of operation is less than 5%. Carrier densities were found to be 1.90×10^{18} and 2.24×10^{16} cm^{-3} for n-type and p-type Cu_2O, respectively. Fermi energies have been calculated, and simplified band structures are constructed. Our results show that Cu_2O is a plausible candidate for both photoanodic and photocathodic electrode materials in photoelectrochemical application.

1. Introduction

Recently the development of environmental friendly, green, and sustainable sources of energy has become a global issue. The use of fossil fuel as a source of energy will not be possible in the near future due to its limited amount and non-renewability. In order to overcome this issue, use of low-cost semiconductor materials for the design of efficient solar convertors is imperative. One possible approach is the use of transition metal oxide (TMO) semiconductor materials in photoelectrochemical (PEC) water splitting to convert solar energy to storable hydrogen energy. Cu_2O is a promising semiconductor material for solar energy conversion with a direct bandgap of 2.0–2.5 eV [1–3] and high-absorption coefficient. Especially, since the conduction and valence bands of Cu_2O are located close to the reduction and oxidation potentials of water, Cu_2O is also a feasible material for the production of hydrogen and oxygen through solar PEC water splitting. Development of simple and economical techniques to deposit photo-active n-type and p-type Cu_2O electrodes is essential for the fabrication of PEC cells or solar cells based on n-Cu_2O/p-Cu_2O homojunction which is expected to achieve devices with high efficiency. Though Cu_2O is a promising material, the development of Cu_2O-based applications is still delayed due to lack of n-type Cu_2O. Recently, both photoanodes and photocathodes are formed from Cu_2O thin films, and the results indicate that Cu_2O is potentially applicable for PEC water splitting [4, 5]. Cu_2O prepared by thermal oxidation or by physical vapor deposition usually contains copper vacancy (V_{Cu}) defects with a carrier density as high as 10^{18} cm^{-3} that results in its p-type conductivity [6]. On the contrary, as our previous report [7] indicates, high-quality n-type Cu_2O material can be deposited by controlling the oxygen flow rates using reactive ion beam sputter deposition (IBSD) in addition to other studies [8–10] done by sputtering and electrodeposition without doping. In this article, we report the demonstration of both n-type and p-type Cu_2O photoelectrodes fabricated by reactive IBSD. Results on conductivity type, photocurrent stability, and carrier densities are presented.

2. Experimental

Cu_2O samples were deposited on quartz substrates in an IBSD chamber [2, 7, 11]. The substrates were cleaned ultrasonically in ethyl alcohol for 10 minutes and then subsequently in deionized water. An air gun with dry nitrogen spray is used to remove all the water droplets and moisture from the surface of the substrates. A metallic copper target (99.99%) was positioned 35 mm downstream of the ion source, and the prepared substrates were placed at 65 mm upstream of the copper target. Two sets of samples with Ar : O_2 flow rates of 4.5 sccm : 0.5 sccm and 4.2 sccm : 0.7 sccm were prepared, where sccm stands for standard cubic centimeter per minute. The samples deposited with Ar : $O_2 = 4.5 : 0.5$ were labeled as Sample 1, while the samples deposited with $Ar : O_2 = 4.2 : 0.7$ were labeled as Sample 2. Both samples were deposited at 450°C for 1.5 hours. The surface morphology of both samples was studied by a field-emission scanning electron microscope (FE-SEM, JEOL JSM-6500F, 15 keV). X-ray photoelectron spectroscopy (XPS) investigation was achieved employing a VG ESCA® Scientific Sigma Probe with Al Kα source at 1486.4 eV. Temperature dependent photoluminescence (PL) properties were characterized from 10 to 300 K using a blue laser at 405 nm with a power of 5 mW as the excitation light source. The spectra were dispersed by a Triax 550 spectrometer and detected by a Symphony CCD detector cooled to −70°C. PEC measurements were carried out utilizing a Gamry G 300 potentiostat with an Ag/AgCl electrode as the reference electrode, Cu_2O samples as the working electrode, and Pt as the counter electrode. During PEC measurement, the Cu_2O samples were attached to a customized electrochemical cell, and a xenon lamp with an intensity of 100 mW/cm^2 was used for illumination. The electrochemical cell was filled with argon purged 0.5 M K_2SO_4 as the electrolyte.

3. Results and Discussion

Figures 1(a) and 1(b) show FE-SEM micrographs of Sample 1 and Sample 2, respectively. From Figure 1(a), Sample 1 exhibits a morphology containing Cu_2O nanorods and small Cu_2O nanostructures. The Cu_2O nanorods exhibit a length of approximately 1 μm and a diameter of ~0.2 μm. As the oxygen flow rate increases, Sample 2 exhibits a smooth thin film surface morphology with tiny nanoparticles on the surface, as shown in Figure 1(b).

Figure 2(a) shows Cu2p core level spectra of both samples. From Figure 2(a), $Cu2p_{3/2}$ and $Cu2p_{1/2}$ binding energy peaks of both samples are located at 932.4 eV and 952.4 eV [12], respectively. The absence of shake-up satellite peaks in the Cu2p spectral around 943 eV and 960 eV indicates the absence of CuO from both Sample 1 and Sample 2. From Figure 2(b), the O1s core level spectra of both samples were deconvoluted into two peaks p1 and p2 located at ~530.5 and ~532.3 eV [12], respectively. The first peak p1 is attributed to oxygen located in ideal metal oxide matrix, while the second peak p2 is attributed to surface adsorbed oxygen or water. The area percentages of p2 in Sample 1 and Sample 2 are 7.8% and 40%, respectively. This indicates that Sample 1 has lower oxygen content that comes from surface adsorbed oxygen or water, indicating a better surface quality. The atomic percentage ratios of Cu : O were calculated and were found to be 64.5 : 35.5 and 62.6 : 37.4 for Sample 1 and Sample 2, respectively. XPS results show that both samples are close to stoichiometric Cu_2O, while higher oxygen flow rate results in higher oxygen atomic percentage.

Figure 3 shows baseline corrected PL spectra of Sample 1 and Sample 2 taken at 10 K. From Figure 3(a), Sample 1 shows a strong PL emission centered at ~1.72 eV, while Sample 2 shows no PL emission peaks at all. As temperature increases, the intensity of 1.72 eV emission decreases while its peak position shifts to lower energy level as temperature is raised to 100 K (Figure 3(b)). The slope of the 1.72 eV peak position emission was found to be -5.2×10^{-4} eV/K, which indicates that this emission is due to the presence of oxygen vacancy defects V_O^{2+} [13]. The PL study shows that Sample 1 contains V_O^{2+} defects only, while no V_{Cu}-related emissions were found, which suggests that Sample 1 is likely to be of n-type conductivity.

Figure 4 demonstrates Tauc's plots which indicate the direct bandgap nature of both samples. From Figure 4, Sample 1 can be characterized with the bandgap at $E1 = 2.3$ eV [14] and Sample 2 can be characterized with the bandgap at $E2 = 2.5$ eV [2]. As clearly seen from Figure 4, Sample 1 shows a strong band tail indicating the presence of subbandgap states (defect states). These defect states are likely due to oxygen vacancy which can be formed ~0.38 eV below the conduction band minimum [15]. From Figure 4, it is clearly seen that the bandgap becomes narrower when the oxygen flow rate decreases.

Figures 5(a) and 5(b) show transient photocurrent properties of Sample 1 under −0.3 V (Figure 5(a)) and +0.3 V (Figure 5(b)) bias relative to Ag/AgCl reference electrode. The result evidently shows that, under negative bias, the sample shows negligible photocurrent. Conversely, when the sample is biased positively, stable anodic photocurrent is observed, demonstrating that Sample 1 is of n-type. Figures 5(c) and 5(d) show transient photocurrent properties of Sample 2 under −0.3 and +0.3 V biases, respectively. When Sample 2 is biased negatively, stable cathodic photocurrent is observed, while under positive bias, it shows almost zero anodic photocurrent. The observation of stable and dominant cathodic photocurrents indicates that Sample 2 is of p-type. The transformation of the carrier type from n-type to p-type when the oxygen flow rate increases indicates that oxygen vacancy defects are the sources of n-type conductivity in Cu_2O as observed from PL data.

Figure 6 shows the linear sweep voltammetry measurement of Sample 1 and Sample 2. Figure 6(a) clearly shows that, in a broad window of measurement voltage, Sample 1 exhibits anodic photocurrent across the whole voltage range and the value increases as the potential becomes more positive. On the contrary, Figure 6(b) shows in the same broad window of measurement voltage, Sample 2 shows cathodic photocurrent across the whole voltage range and the value increases as the potential becomes more negative. This observation of n-type conductivity form Sample 1 and p-type conductivity from Sample 2 is consistent with transient photocurrent characterization results.

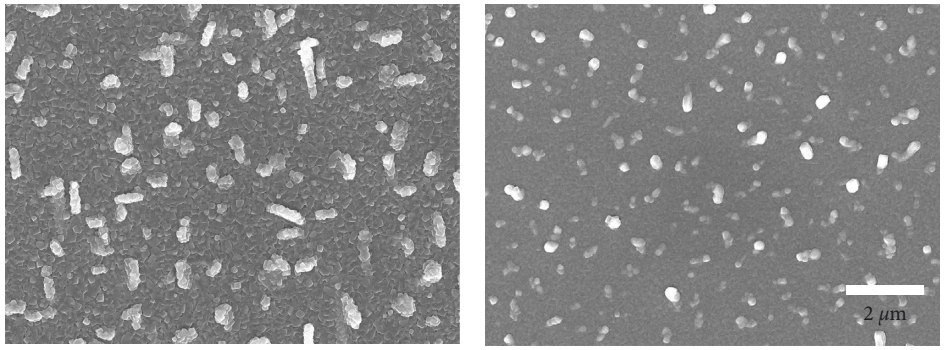

Figure 1: FE-SEM micrographs of (a) Sample 1 and (b) Sample 2.

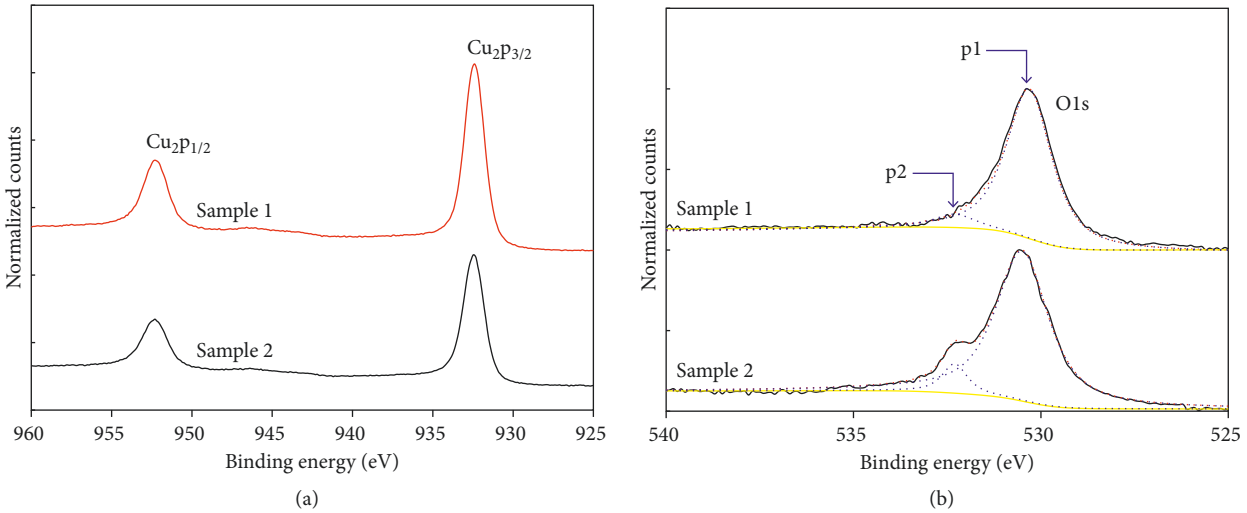

Figure 2: High-resolution XPS spectra for (a) Cu2p and (b) O1s core levels. The O1s spectra are deconvoluted into two Gaussian peaks p1 (blue dotted line) and p2 (blue dotted line). The summation of these two curves (red dotted line) shows the perfect fit to the measured result (black solid line) and the curve with yellow dotted line shows the baseline.

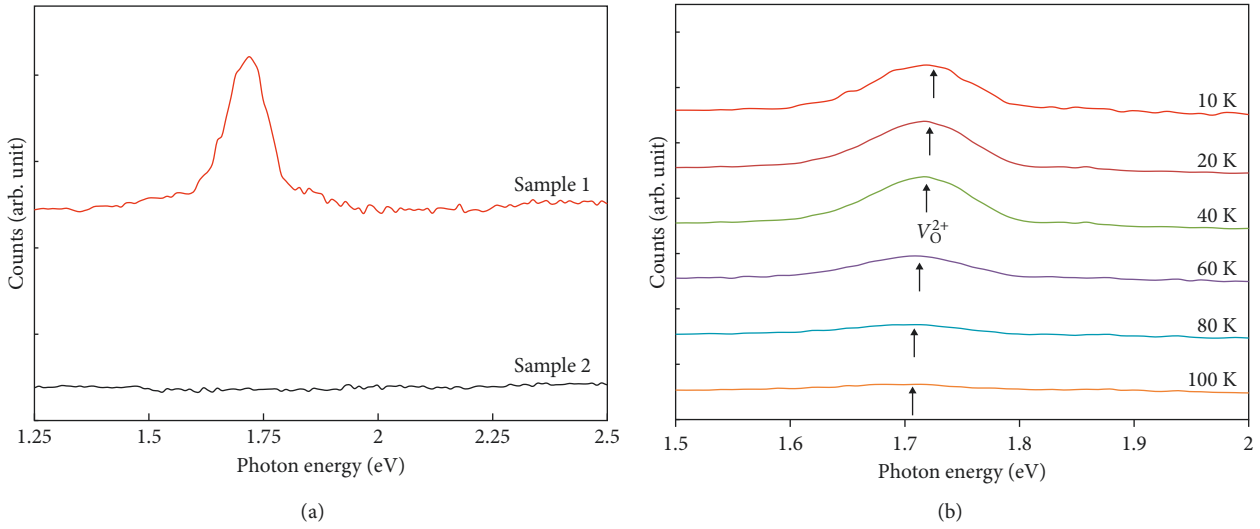

Figure 3: (a) PL spectra of Sample 1 and Sample 2 at 10 K. (b) Temperature-dependent peak position of the 1.72 eV emission of Sample 1.

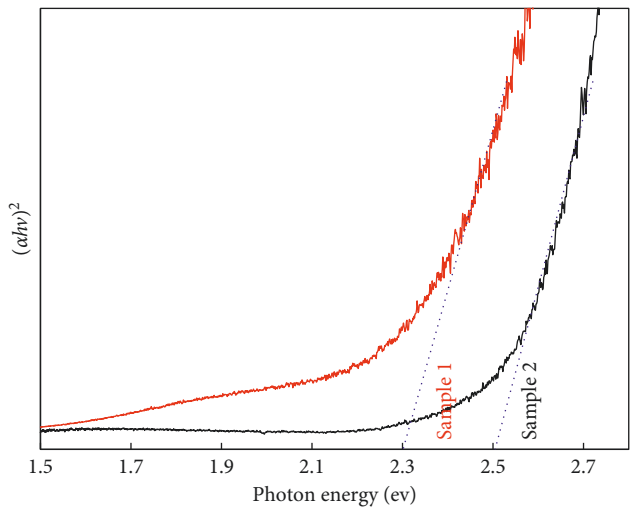

FIGURE 4: Tauc's plots of Sample 1 (red line) and Sample 2 (black line).

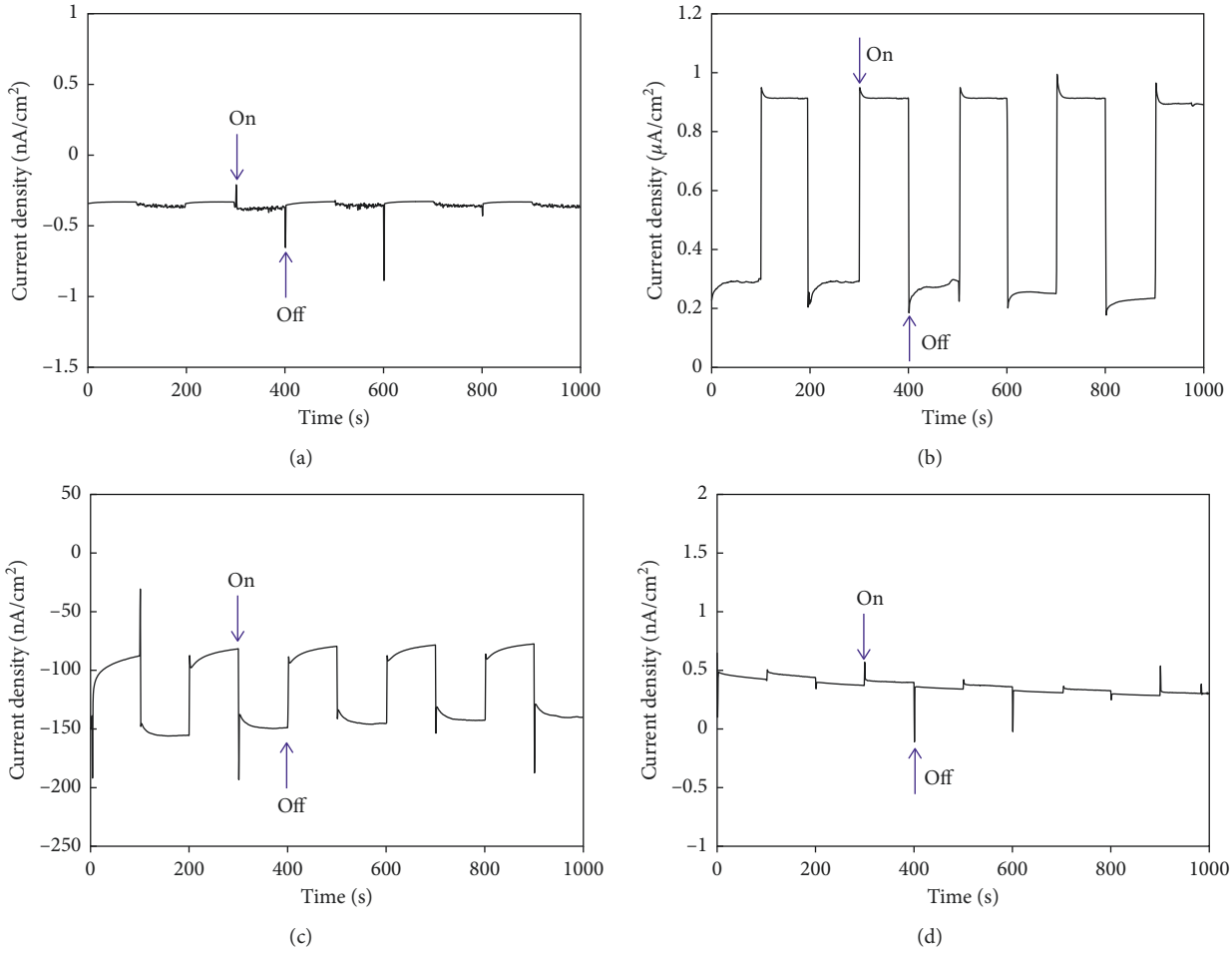

FIGURE 5: Transient photocurrent properties of Sample 1 biased at (a) −0.3 V and (b) +0.3 V relative to Ag/AgCl reference electrode. Transient photocurrent properties of Samples 2 biased at (c) −0.3 V and (d) +0.3 V relative to Ag/AgCl reference electrode.

From Figure 7(a), the Mott–Schottky plot of Sample 1 shows the n-type nature of the photoelectrode since the value of the slope is positive. However, the Mott–Schottky plot of Sample 2 shows typical behavior of p-type electrode since the value of the slope of the slope is negative. The result of the slopes of the Mott–Schottky plots of Cu_2O electrodes

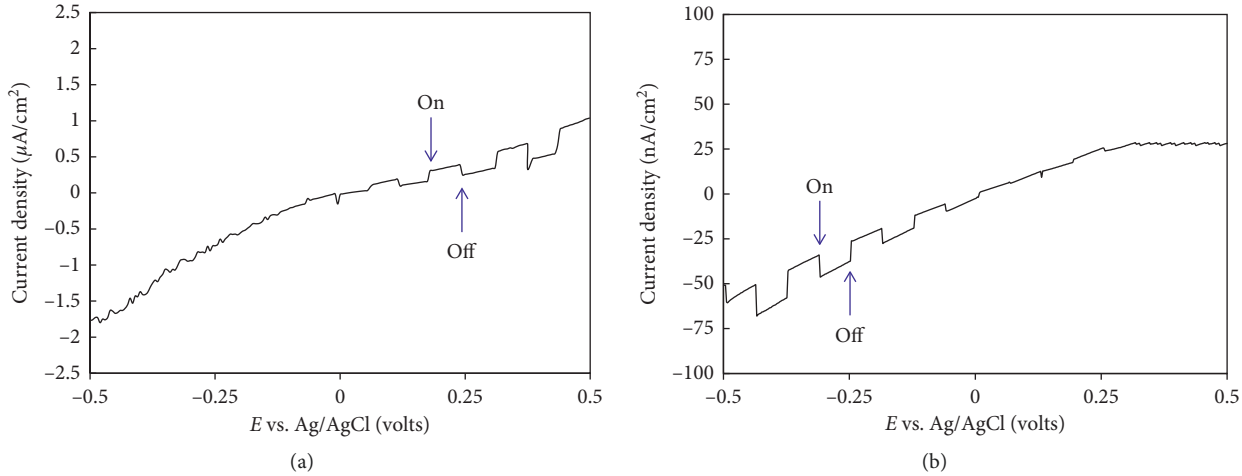

Figure 6: Linear sweep voltammetry measurements for (a) Sample 1 and (b) Sample 2.

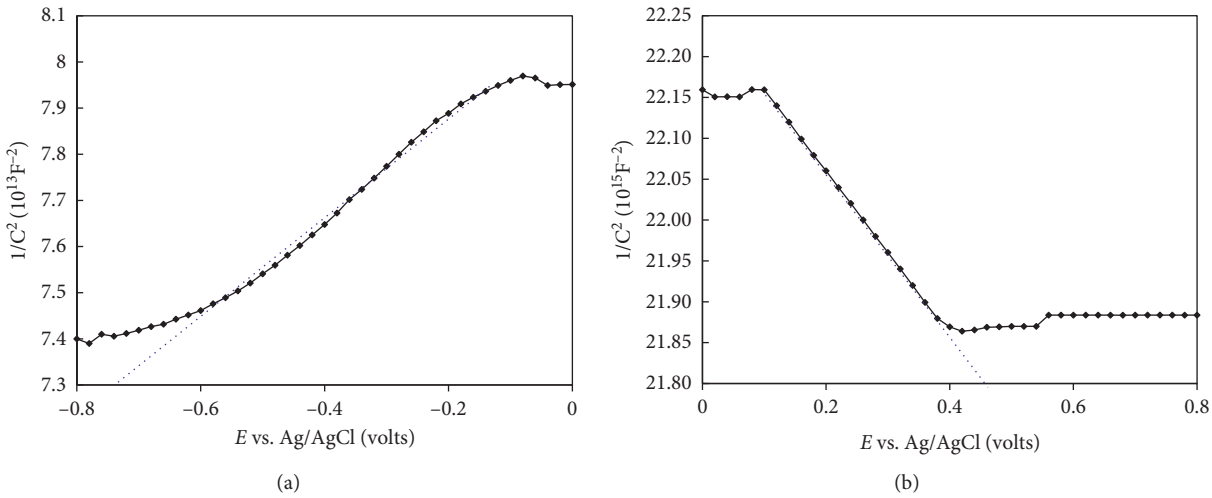

Figure 7: The Mott–Schottky plots of Cu_2O electrodes (a) Sample 1 and (b) Sample 2 measured at 10 kHz.

is an additional confirmation of carrier types investigated by using both the photocurrent and linear sweep voltammetry measurement. The acceptor and donor densities can be calculated employing the Mott–Schottky equations [16]:

$$\frac{1}{C_{SC}^2} = \pm\frac{2}{\varepsilon\varepsilon_0 N}\left(V - V_{FB} - \frac{k_B T}{e}\right), \quad (1)$$

where the negative sign is for p-type and positive sign for n-type conductivity, N is the charge carrier density, donor density (N_D) for n-type or acceptor density (N_A) for p-type semiconductors, C_{SC} represents the capacitance of the space charge region, ε is the relative dielectric constant of Cu_2O which equals to 6.3 [17], and V is the applied electrode potential (volts). The carrier densities can thus be estimated using the following equation:

$$N = \frac{2}{e\varepsilon\varepsilon_0}\frac{1}{d/dV\left(1/C_{SC}^2\right)}. \quad (2)$$

N_D and N_A calculated using data from Figures 7(a) and 7(b) were found to be $1.90\times10^{18}\,cm^{-3}$ and $2.24\times10^{16}\,cm^{-3}$ for Sample 1 and Sample 2, respectively. The higher carrier concentration of Sample 1 implies a faster charge transfer and then an enhanced PEC performance [18]. Furthermore, from the intercept of the Mott–Schottky plots, the flat band potentials (V_{fb}) for Sample 1 and Sample 2 are −0.73 and 0.42 V versus the reference electrode, respectively. The calculated flat band potentials of both samples are almost consistent with the previous reports [5, 10, 19, 20]. The more negativity and positivity of the flat band potentials of the photoanode and photocathode are essential since the higher the flat band potential results higher band bending and larger space charge region potentials in the semiconductor/electrolyte interfaces.

To explain the use of the two electrodes for water reduction and oxidation, simplified band diagrams of both samples are constructed. Since Sample 1 is n-type, the Fermi level E_F position of Sample 1 is calculated using

$$E_{CB} - E_F = \frac{k_B T}{e} \ln \frac{N_C}{N_D}, \quad (3)$$

where E_{CB} is the conduction band minimum of Sample 1. In Equation (3), N_D is the density of donor which can be approximated as the density of electrons which equals to $1.90 \times 10^{18}\,\mathrm{cm}^{-3}$. N_C is the effective density of state in the conduction band which can be found as

$$N_C = 2\left(\frac{2\pi m_e^* k_B T}{h^2}\right)^{3/2}, \quad (4)$$

where m_e^* is the effective mass of electrons which equals to $0.99\,m_0$ [21]. The calculation result shows that the Fermi energy level of Sample 1 is at 0.3 eV below conduction band minimum. Similar calculation is carried out for Sample 2 using the following equation:

$$E_F - E_{VB} = \frac{k_B T}{e} \ln \frac{N_V}{N_A}, \quad (5)$$

where E_{VB} is the valance band maximum and N_V is the effective density of state in the the valance band of Sample 2 which can be found as

$$N_V = 2\left(\frac{2\pi m_p^* k_B T}{h^2}\right)^{3/2}. \quad (6)$$

By taking the approximation that N_A equals to hole density and that the effective mass of the hole in Cu_2O is $0.58\,m_0$ [21], the Fermi energy position of Sample 2 was found to be 0.9 eV above the valance band maximum.

Figure 8 shows simplified band diagrams of Sample 1 and Sample 2 with energy scales relative to both vacuum and normal hydrogen electrode (E_{NHE}). From Figure 8, it shows that the band structures of both samples remain approximately unchanged, while the only difference is the location of the Fermi energy level. One important issue in PEC cell technology is to find semiconductor photoelectrodes that can absorb the visible light and drive hydrogen (oxygen) evolution reaction using the photogenerated electrons (holes). This needs the semiconductor to have proper band alignment relative to the water redox potentials. From Figure 8, it can be found that E_F of Sample 1 (n-type) is at 0.1 eV above $E_{NHE} = 0$, indicating that Sample 1 is suitable to act as a photoanode material. Also from Figure 8, E_F of Sample 2 (p-type) is at 1.1 eV below $E_{NHE} = 0$, indicating that Sample 2 is suitable to act as photocathode. This demonstrates that, by controlling argon/oxygen flow rates, Cu_2O deposited by reactive IBSD is suitable to act as both photoanode and photocathode in PEC water splitting applications.

4. Conclusion

Cu_2O with novel optical properties and PEC activities has been deposited successfully by reactive IBSD by controlling the argon/oxygen flow rates. PL study shows that n-type Cu_2O is due to the presence of oxygen vacancy defects. We demonstrated the bandgap position alignments of the two photoelectrodes with respect to the reduction and oxidation of water, and the result shows that both samples are promising for PEC water splitting applications.

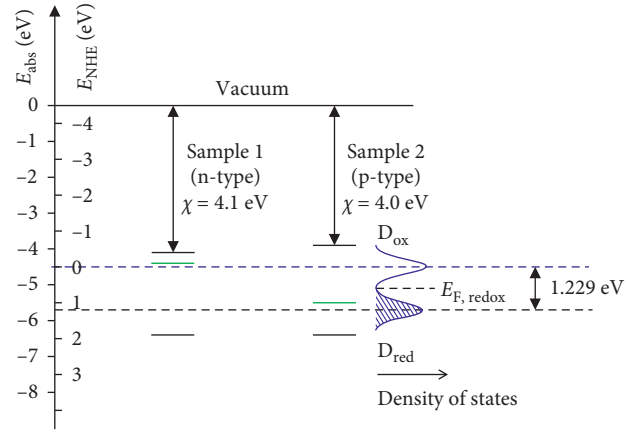

Figure 8: Energy band scheme for n-type (Sample 1) and p-type (Sample 2) Cu_2O electrodes with respect to both vacuum and NHE levels. The Fermi levels of both samples are labeled as green lines.

Data Availability

Data supporting this research article are available from the corresponding author upon reasonable.

Conflicts of Interest

The authors declare that they have no conflicts of interest.

Acknowledgments

This research work was supported by the Ministry of Science and Technology of Republic of China under contract number MOST 107-2221-E-011-084.

References

[1] L. O. Grondahl, "The copper-cuprous-oxide rectifier and photoelectric cell," *Reviews of Modern Physics*, vol. 5, no. 2, pp. 141–168, 1933.

[2] M. J. Hong, Y. C. Lin, L. C. Chao, P. H. Lin, and B. R. Huang, "Cupric and cuprous oxide by reactive ion beam sputter deposition and the photosensing properties of cupric oxide metal-semiconductor-metal Schottky photodiodes," *Applied Surface Science*, vol. 346, pp. 18–23, 2015.

[3] L. Zhang, L. McMillon, and J. McNatt, "Gas-dependent bandgap and electrical conductivity of Cu_2O thin films," *Solar Energy Materials and Solar Cells*, vol. 108, pp. 230–234, 2013.

[4] Q. B. Ma, J. P. Hofmann, A. Litke, and E. J. M. Hensen, "Cu_2O photoelectrodes for solar water splitting: tuning photoelectrochemical performance by controlled faceting," *Solar Energy Materials and Solar Cells*, vol. 141, pp. 178–186, 2015.

[5] J. Luo, L. Steier, M. K. Son, M. Schreier, M. T. Mayer, and M. Grätzel, "Cu_2O Nanowire photocathodes for efficient and durable solar water Splitting," *Nano Letters*, vol. 16, no. 3, pp. 1848–1857, 2016.

[6] T. Ito and T. Masumi, "Detailed examination of relaxation processes of excitons in photoluminescence spectra of Cu_2O,"

Journal of the Physical Society of Japan, vol. 66, no. 7, pp. 2185–2193, 1997.

[7] A. A. Ejigu and L. C. Chao, "Characterization of n-type Cu_2O deposited by reactive ion beam sputter deposition," *Journal of Vacuum Science & Technology B, Nanotechnology and Microelectronics: Materials, Processing, Measurement, and Phenomena*, vol. 35, no. 6, article 061205, 2017.

[8] D. Cao, C. Wang, F. Zheng, W. Dong, L. Fang, and M. Shen, "High-efficiency ferroelectric-film solar cells with an n-type Cu_2O cathode buffer layer," *Nano Letters*, vol. 12, no. 6, pp. 2803–2809, 2012.

[9] K. Han and M. Tao, "Electrochemically deposited p–n homojunction cuprous oxide solar cells," *Solar Energy Materials and Solar Cells*, vol. 93, no. 1, pp. 153–157, 2009.

[10] P. Wang, H. Wu, Y. Tang, R. Amal, and Y. H. Ng, "Electrodeposited Cu_2O as photoelectrodes with controllable conductivity type for solar energy conversion," *Journal of Physical Chemistry C*, vol. 119, no. 47, pp. 26275–26282, 2015.

[11] C. H. Chen, Y.-L. Huang, K. Huang, E. A. Ayalew, L. C. Chao, and J. P. Ao, "Controlled oxidation state of silver oxide thin films deposited by an integrated anode layer ion source ion beam sputter module," *Nuclear Instruments and Methods in Physics Research Section B: Beam Interactions with Materials and Atoms*, vol. 412, pp. 41–45, 2017.

[12] Y. Wang, J. Im, J. W. Soares, D. M. Steeves, and J. E. Whitten, "Thiol adsorption on and reduction of copper oxide particles and surfaces," *Langmuir*, vol. 32, no. 16, pp. 3848–3857, 2016.

[13] R. Garuthara and W. Siripala, "Photoluminescence characterization of polycrystalline n-type Cu_2O films," *Journal of Luminescence*, vol. 121, no. 1, pp. 173–178, 2006.

[14] I. Mukherjee, S. Chatterjee, and N. A. Kulkarni, "Band gap tuning and room-temperature photoluminescence of a physically self-assembled Cu_2O nanocolumn array," *Journal of Physical Chemistry C*, vol. 120, no. 2, pp. 1077–1082, 2016.

[15] K. Matsuzaki, K. Nomura, H. Yanagi, T. Kamiya, M. Hirano, and H. Hosono, "Effects of post-annealing on (110) Cu_2O epitaxial films and origin of low mobility in Cu_2O thin-film transistor," *Physica Status Solidi A*, vol. 206, no. 9, pp. 2192–2197, 2009.

[16] P. K. Pagare and A. P. Torane, "Band gap varied cuprous oxide (Cu_2O) thin films as a tool for glucose sensing," *Microchimica Acta*, vol. 183, no. 11, pp. 2983–2989, 2016.

[17] L. Wang and M. Tao, "Fabrication and characterization of pn homojunctions in cuprous oxide by electrochemical deposition," *Electrochemical and Solid-State Letters*, vol. 10, no. 9, pp. H248–H250, 2007.

[18] M. Ye, J. Gong, Y. Lai, C. Lin, and Z. Lin, "High-efficiency photoelectrocatalytic hydrogen generation enabled by palladium quantum dots-sensitized TiO_2 nanotube arrays," *Journal of the American Chemical Society*, vol. 134, no. 38, pp. 15720–15723, 2012.

[19] C. Li, Y. Li, and J. J. Delaunay, "A novel method to synthesize highly photoactive Cu_2O microcrystalline films for use in photoelectrochemical cells," *ACS Applied Materials & Interfaces*, vol. 6, no. 1, pp. 480–486, 2014.

[20] C. M. McShane and K. S. Choi, "Photocurrent enhancement of n-type Cu_2O electrodes achieved by controlling dendritic branching growth," *Journal of the American Chemical Society*, vol. 131, no. 7, pp. 2561–2569, 2009.

[21] J. W. Hodby, T. E. Jenkins, C. Schwab, H. Tamura, and D. Trivich, "Cyclotron resonance of electrons and of holes in cuprous oxide, Cu_2O," *Journal of Physics C: Solid State Physics*, vol. 9, no. 8, pp. 1429–1439, 1976.